Insight of an easy topochemical oxidative reaction in obtaining high performance electrochemical capacitor based on CoIICoIII monometallic cobalt Layered Double Hydroxide

Pierre Vialat, Pierre Rabu, Christine Mousty, Fabrice Leroux

Insight of an easy topochemical oxidative reaction in obtaining high performance electrochemical capacitor based on $Co^{II}Co^{III}$ monometallic cobalt Layered Double Hydroxide

Pierre Vialat [a], Pierre Rabu [b, c], Christine Mousty [a], Fabrice Leroux [a, *]

[a] *Université Clermont Auvergne, Université Blaise Pascal, Institut de Chimie de Clermont-Ferrand, UMR-CNRS 6296, F-63000 Clermont-Ferrand, France*
[b] *Institut de Physique et Chimie des Matériaux de Strasbourg (IPCMS) (UMR7504 CNRS – Université de Strasbourg), 23 Rue du Loess, F-67034 Strasbourg, France*
[c] *International Center for Frontier Research in Chemistry (icFRC), 8, Allée Gaspard Monge, F-67000 Strasbourg, France*

A series of monometallic Layered Double Hydroxides (LDH) using electroactive cation, i.e. divalent or trivalent cobalt, was prepared by Topochemical Oxidation Reaction (TOR) under O_2 atmosphere at 40 °C from pristine β-$Co(OH)_2$ platelets. The oxidation state of the ill-defined layered materials was evaluated by coupling thermal measurements and chemical titration (iodometry). Their characterization by ancillary techniques was completed by the study of their magnetic behavior. The obtained magnetic moments suggest the presence of structural local deformation around the Co^{II} ions, unhomogeneous charge distribution yielding to clustering effects cannot be discarded. Their pseudo-faradic properties as supercapacitor in KOH solution was thoroughly investigated by using Cyclic Voltammetry (CV), Galvanostatic Cycling with Potential Limitation (GCPL) and Electrochemical Impedance Spectroscopy (EIS) techniques. As a function of the oxygen treatment, the relative amount of Co^{II}/Co^{III} was found to range into 5.3 and 13.3, which is unusually high when compared to classical LDH charge distribution. Pseudocapacitance as high as 1540 F g^{-1} was obtained underlining a high percentage of Co^{II}, ≈40%, involved in electrochemical process. This high percentage is tentatively explained by an extended outer-active electrochemical surface which demonstrates that TOR is a quick and easy process to get a high pseudocapacitive performance.

* Corresponding author.
E-mail address: fabrice.leroux@univ-bpclermont.fr (F. Leroux).

1. Introduction

Electrochemical capacitors, so-called "supercapacitors", delivering usually a high power density in a very short time, may be classified in energy storage by electron process. Thus, according to the mechanisms involved, one distinguishes the so-called "electrochemical double-layer capacity" (as illustrated by carbon materials) which is occurring at the vicinity of the surface of electrode materials and/or the so-called "pseudo-capacity" which may involve fast faradic multi-electron-transfer reactions (such as with metal oxides/hydroxides [1]). Among other parameters, the power associated to the reversibility and the stability during cycling is known to mostly determine the overall performances of pseudocapacitors.

Among possible inorganic frameworks found to exhibit appealing pseudo-capacitive properties, Layered Double Hydroxides (LDH) composed of electroactive metal cations, have been recently reported as interesting candidates. For instance, various LDH compositions, CoAl-LDH and CoNiAl-LDH were found to exhibit high capacitance, ranging from 500 to 1000 F g^{-1} [1,2]. To further improve their electrochemical performances, the textural morphology was modified using microwave assisted synthesis [3,4] or electrodeposition methods [5,6]. CoFe LDH compound was recently reported to exhibit magnetic and good energy storage properties [7]. Additionally, composites were elaborated deriving from nanocarbons and LDH combining the capacitive properties of both components [8–12]. In order to further improve the capacity, electroactive mono cation LDH is desired, without Al spectator. Indeed, recently, we prepared a monometallic $Co^{II}_xCo^{III}$-CO_3 LDH by *in situ* oxidative reaction [13], adapted from the protocol described by Xu and Zeng [14,15], probably thanks to a topochemical reaction between β-$Co(OH)_2$ and LDH structures related through their lamellar character. The chemical composition of LDH is represented by the general formula $[M^{II}_{1-a}M^{III}_a(OH)_2]^{x+}[(A^{n-})_{a/n}, y\ H_2O]$ (abbreviated as $M^{II}_1M^{III}_2$-A), where M^{II} is a divalent metal cation (here Co^{II}) and M^{III} is a trivalent metal (here Co^{III}), and A^{n-} is the interlayer anion compensating the positive charge of the metal hydroxide layers. The Topochemical Oxidative Reaction (TOR) between β-$Co(OH)_2$ and LDH was found to proceed under air after a rather long experiment time (t ≈ 3 days). In order to circumvent this time condition as well as to relate the chemical composition to the observed electrochemical performance, we performed a more rapid oxidation using oxygen during various times of exposure. The TOR reaction was carried out long enough to convert more than 10% of Co^{II} into Co^{III}.

Therefore, we present here a series of LDH phases containing different amounts of Co^{II} and Co^{III} cations which were prepared using a TOR under pure O_2 atmosphere instead of air as the oxidizing agent. The new solids were prepared by varying the oxidation time and were characterized by powder X-ray Diffraction (XRD). The Co^{III} content was determined by coupling Thermo-Gravimetric Analysis (TGA) along with iodometric titration of the Co^{III} species. Their magnetic behavior was investigated as a function of field and temperature. Their electrochemical characteristics were evaluated by Cyclic Voltammetry (CV) and Electrochemical Impedance Spectroscopy (EIS) in 0.1 M KOH. Their capacitive properties were finally determined using Galvanostatic Cycling with Potential Limitation (GCPL) analysis at different current densities varying from 0.5 to 50 A g^{-1} for charge and discharge and displayed into Ragone diagrams. The electrochemical properties are discussed on the basis of the chemical composition of the oxidation of the LDH phases (i.e. the Co^{III}/Co_{tot} ratio).

2. Experimental

2.1. Material synthesis

A series of $Co^{II}_xCo^{III}$-LDH with *x* representing the Co^{II}/Co^{III} ratio was synthesized by TOR under oxygen atmosphere. Typically, 25 mL of 0.1 M $Co(NO_3)_2 \cdot 6H_2O$ (Acros, 99%) solution was quickly added in 200 mL of 0.5 M NH_4OH solution (Acros, 28–30% wt. in water) in a three-necked round bottom flask. Pure O_2 (Saga, France) was introduced immediately by bubbling in the stirred solution and the color of the suspension was found to change from pink to brownish green after very short time (seconds). It is noteworthy that the color remained pink under nitrogen, *i.e.* in absence of O_2 bubbling evidencing formation of β-$Co(OH)_2$ in absence of oxidizing agent (further confirmed by XRD). The reaction temperature was kept at 40 °C during the whole experiment by varying the time of oxidation $0.5 \leq T_{O2} \leq 8$ h. It should be noted that for longer O_2 bubbling time ($T_{O2} > 8$ h), the formation of Co^{III} containing impurities (CoOOH) was observed. The molar ratio of ammonium hydroxide to Co^{II} nitrate was close to 40, in favor of soluble amine Co^{II} complexes formation. This may explain the relatively small reaction yield (20% by wt.) when comparing the obtained and expected product quantities. The precipitates were finally recovered by centrifugation at 4500 rpm for 5 min, washed three times with deionized water and dried in an oven overnight at 30 °C. A reference product to estimate the efficiency of the O_2 treatment was prepared following the same protocol but under air oxidizing atmosphere for 60 h [13].

2.2. Material characterizations

The oxidation rate of Co^{II} to Co^{III} was evaluated by coupling TGA measurements along with iodometric titrations of Co^{III} as already reported by Xu and Zeng [14,15]. Experimentally, the total Co content and associated formula weight were determined by TGA analysis considering that only Co_3O_4 was obtained above 600 °C, as confirmed by XRD analysis of the residual product. TGA analyses were carried out with a Setaram 92-16.16 balance under air flow in the temperature range 25–1100 °C with a linear temperature ramp of 5 °C per min. The Co^{III} content was determined by a redox reaction: 20 mg of LDH phases were dissolved in an acidified 0.1 M KI solution and Co^{III} cations reduced to Co^{II} by reaction with I^- anions following the reaction:

$$Co^{III} + I^- \rightarrow \tfrac{1}{2}\, I_2 + Co^{II}$$

The formed di-iodine was titrated by UV spectroscopy at its maximum peak absorption of 352 cm^{-1} ($\varepsilon = 12{,}000\ cm^{-1}\ L^{-1}$ mol). The analysis was realized on a Nicolet Evolution 500 from Thermo Scientific between 200 and 500 cm^{-1}.

Powder X-Ray Diffraction (PXRD) measurements were performed using a Siemens D501 diffractometer in Bragg-Brentano geometry with Cu-$K_{\alpha 1}/_{\alpha 2}$ radiation. Data were collected between 4.0 and 70.0 2θ (°), with a step size of 0.08 2θ (°) and a counting time of 3 s/step.

SEM analyses were made using a Zeiss Supra 55 VP with an acceleration voltage of 3 kV at different magnifications. The samples were prepared by deposition of a small amount of powders onto carbon support and metallized using Au to enhance electron conductivity.

Cyclic Voltammetry (CV), Galvanostatic Cycling with Potential Limitation (GCPL) and Electrochemical Impedance Spectroscopy (EIS) measurements were carried out using a BioLogic Science

Instruments SP-150. The experiments were performed in a 0.1 M KOH (Sigma–Aldrich) solution using a three-electrode cell, including a saturated calomel electrode (SCE) as reference electrode, a platinum auxiliary electrode and the platinum electrode (A = 0.07 cm^2) coated with LDH oxidative phases thin films as working electrode. Before deposition, the Pt surface was polished with 1 μm-diamond paste and washed with acetone and then polished again with 0.05 μm alumina slurry then rinsed with water and ethanol. 10 μL of an overnight stirred 2 mg mL^{-1} LDH suspension (20 μg) was deposited onto Pt electrode and dried in air. The films were found to have a thickness of around 1 μm.

CV measurements were recorded at a sweep rate (v) of 5 mV s^{-1} over a potential window from −0.2–0.5 V/SCE. GCPL experiments were recorded over a potential window from 0 to 0.45 V/SCE for charge experiments and from 0.45 to 0 V/SCE for discharge experiments. The current densities employed were 0.5, 1.0, 2.0, 5.0, 10.0, 20.0 and 50.0 A g^{-1}. The current was calculated for a quantity of 20 μg of active LDH deposit on the platinum electrode. The charge and discharge capacities were determined using the formula:

$$C = \frac{I \cdot \Delta t}{m \cdot \Delta V}$$

Ragone charts were plotted calculating power density and energy density according to the formulae:

$$E = \frac{\Delta V \cdot I \cdot \Delta t}{m} \text{ and } P = \frac{\Delta V \cdot I}{m}$$

EIS measurements were recorded at the Open Circuit Potential (OCP) after oxidation cycling (ten cycles). A sinusoidal potential modulation with amplitude of 10 mV (peak to peak) was applied with a frequency from 25 mHz–100 kHz. The obtained Nyquist plots were fitted with ZView software to determine parameters value of an appropriate equivalent circuit chosen from the literature [16].

DC and AC magnetic measurements were carried out with an S-VSM Quantum design Squid VSM set-up with applied DC field in the range −7 T to +7 T and temperature varying between 1.8 K and 300 K. The temperature variation of the magnetic susceptibility was recorded under a DC field of 500 Oe. An AC field of 3.5 Oe at 83 Hz was used for measuring the temperature dependence of the real and imaginary parts of the magnetic susceptibility. All data were corrected for diamagnetism of the samples and of the sample holder (gel caps).

3. Results

3.1. Chemical and structural characterization

$Co^{II}_xCo^{III}$-LDH with x representing Co^{II}/Co^{III} were prepared by a topochemical and oxidative reaction (TOR) adapted from the publications of Xu and Zeng [14,15]. This reaction proceeds by *in situ* oxidation under pure oxygen atmosphere of some Co^{II} cations into β-$Co(OH)_2$ pristine phase. Preferably, such straightforward procedure was applied instead of an oxidation by Br_2 as reported by Ma and al [17]. because of the difficult handling of Br_2. Another synthesis route using microwaves to oxidize cobalt was also reported by Zapataa et al. [18] but leads to materials with a very poor crystallinity.

From elemental analysis, different Co^{III}/Co_{tot} atomic ratios (%) were determined depending on the reaction time, T_{O2} (Table 1). The relative Co^{III} content was found to increase with oxidation time. A steep increase was observed for short T_{O2} to reach a value of about 12% after 2 h. Then the Co^{III} % slightly increases to a value of 16% after 8 h (Fig. 1). The oxygen treatment with T_{O2} = 0.5 h and 8 h yields a Co^{II}/Co^{III} ratio (x) ranging between 13.3 and 5.3 respectively. Such values are highly unusual for LDH composition regarding the distribution of charge (i.e. M^{III}), as M^{II}/M^{III} ratios between 2 and 4 are classically obtained. However it is noteworthy that low charge density was obtained in a series of Ga-containing hydrotalcite-like materials with Mg/Ga varying between 12.9 and 1.8 [19].

Table 1
Chemical compositions of the as-prepared $Co^{II}_xCo^{III}$ LDH.

T_{O2} (h)	Co^{III}/Co_{tot} (%)[a]	n (H_2O)[b]	Formula
0.5	7	9.6	$Co^{II}_{13.3}Co^{III}(OH)_{28.6}(CO_3)_{0,5}$, 9.6 H_2O
1	10	6.3	$Co^{II}_{9.0}Co^{III}(OH)_{20.0}(CO_3)_{0,5}$, 6.3 H_2O
2	12	5.9	$Co^{II}_{7.3}Co^{III}(OH)_{16.6}(CO_3)_{0,5}$, 5.9 H_2O
4	13	4.9	$Co^{II}_{6.7}Co^{III}(OH)_{15.4}(CO_3)_{0,5}$, 4.9 H_2O
6	14	4.1	$Co^{II}_{6.1}Co^{III}(OH)_{14.2}(CO_3)_{0,5}$, 4.1 H_2O
8	16	3.8	$Co^{II}_{5.3}Co^{III}(OH)_{12.6}(CO_3)_{0,5}$, 3.8 H_2O

[a] Calculated by coupling TGA and iodometric titration.
[b] Calculated from TGA.

The powder X-ray diffraction patterns of the samples displayed in Fig. 2 were consistent with the formation of an LDH phase indexed in the rhombohedral space group R-3m (three-layer polytype). The positions of the 00l (l = 3n) diffraction lines in the low angle region (10–30°/2θ) related to the interlamellar distance ($d_{spacing}$ = n*d_{00l} ≈ 7.80 Å, Table 2) were consistent with the presence of intercalated carbonate anions [20] to compensate the positive charge created by the oxidation of the Co^{II} ions (Table 1). In spite of O_2 bubbling, it is interesting to note that a nitrate LDH phase is not formed (expected basal spacing of about 8.6 Å) but rather a carbonate phase. This can be explained by the fact that TOR is applied under open air exposure. The values of a and c cell parameters were calculated from the position of the (003) and (110) reflections (Table 2). The (110) reflection is characteristic of the intralayer organization and the cell parameter a can be deduced from the relation $a = 2d_{110}$, corresponding to the averaged distance between two nearest metal cations within the hydroxide layer. An average value of a was found around 3.08 Å, consistent with the LDH layer structure [21]. The Co^{III} ionic radius is lower than that of Co^{II} (0.63 Å *vs* 0.72 Å) and an increasing amount of Co^{III} should have led to a decrease in the Co–Co distance that is however not obvious here. The quasi constant value of the a parameter reported in

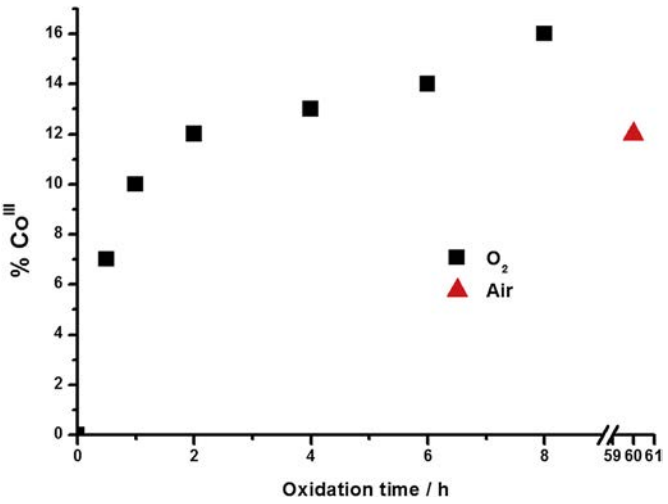

Fig. 1. Evolution of percentage of Co^{III} in $Co^{II}_xCo^{III}$ LDH as a function of oxidation time in O_2 atmosphere.

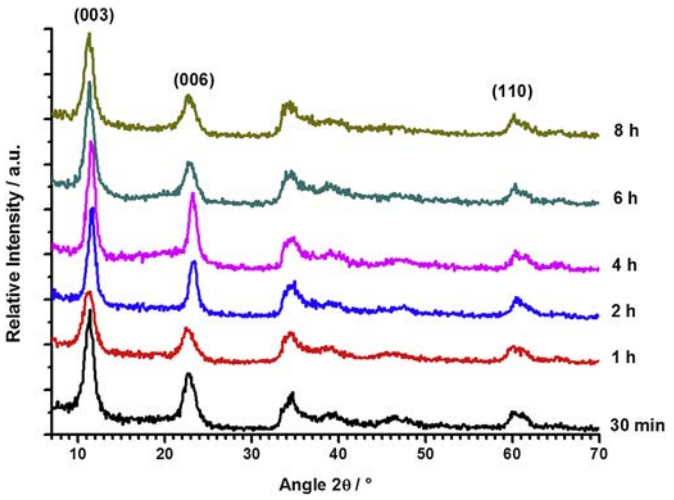

Fig. 2. XRD patterns of the $Co^{II}_{x}Co^{III}$ LDH as a function of oxidation time in O_2 atmosphere.

Table 2 can be explained by the relatively low amounts of Co^{III} together with a low accuracy on the position of the (110) peak due to poor crystallinity in these LDH samples.

3.2. Magnetic properties

The magnetic properties of the present compounds were investigated. The magnetic data are presented in Supporting Information. Since all samples exhibit similar features, we present here the case of $Co^{II}_{6.7}Co^{III}$-LDH ($T_{O2} = 4$ h). The thermal variation of the magnetic susceptibility recorded under a field of 500 Oe is presented in Fig. 3a. The magnetic susceptibility increases continuously between room temperature and 1.8 K, to saturate at 8 $cm^3\ mol^{-1}$. The χT product is almost constant around 20.1 $K\ cm^3\ mol^{-1}$ between 300 K and 150 K. Then a slight minimum is observed followed by a steep increase of the moment up to a maximum of 55 $K\ cm^3\ mol^{-1}$ at 7 K. The high temperature behavior is characteristic of high spin Co^{II} in octahedral field [22–26]. The fit of the inverse susceptibility to the Curie Weiss law, in Fig. 3b, leads to a Curie constant $C = 20.2\ K\ cm^3\ mol^{-1}$ and a small Weiss temperature $\theta = 8.3$ K. Assuming that the six coordinated Co^{III} ions are in the low spin state (S = 0) [27–29], the C value corresponds to 3 $K\ cm^3\ mol^{-1}$ per Co^{II}, which is in the expected range for high spin (S = 3/2, L = 1) Co^{II} ions [22,23,30]. The minimum around 60 K is the signature of spin–orbit coupling effect, although antiferromagnetic interactions cannot be ruled out. The steep increase and the maximum of χT suggest a ferromagnetic ordering which is confirmed by the occurrence of an out of phase signal in the AC susceptibility *vs* T measurement, showed in Fig. 3d. The ordering temperature $T_C = 7.8$ K can be deduced from the maximum of $\chi'(T)$. It is worth noting that $\chi''(T)$ does not exhibit a single peak, a shoulder being observed towards the low temperatures. This suggests the presence of two different magnetic phases that can ascribe for disorder, inhomogeneous water content or inhomogeneous cation distribution [31,32]. Consistently, the zero field cooled (ZFC) and the field cooled (FC) susceptibilities (Fig. 3c) split below T_C. The maximum of the ZFC curve occurs very close to T_C and the FC curve continues to increase below T_C to its saturation value of 54 $cm^3\ mol^{-1}$. This behavior is typical of ferromagnetic ordering. In particular, there is no sign of spin-glass phase which would be characterized by a plateau below T_C. Finally, long range magnetic ordering is supported by the magnetization versus field hysteresis curve at 1.8 K, in Fig. 3e. One observes a coercive field of 602 Oe and a saturation *vs* magnetization Ms = 13.2 μ_B at 7 T. The later corresponds to 2 μ_B per Co^{II} which is in the lower range of values for six-coordinated Co^{II} ions in hydroxides [22,24,30,33,34].

The characteristic data for all compounds are presented in Table 3. Although the general behavior is very alike for the whole series, some discrepancies in the characteristic values *C*, θ, and *Ms* can be denoted. It seems that there is no regular variation with the amount of magnetic ions in the structure. Moreover, the magnetic moments per ions are relatively lower than in $Co^{II}_{6.7}Co^{III}$-LDH ($T_{O2} = 4$ h) and lower than expected when comparing with the literature [22,24,30,33,34]. All values were deduced based on the iodometric titration of the Co^{III} ions which can suffer some errors. Another possible suggestion to explain these low values is that the presence of Co^{III} can induce significant deformation of the structure around the Co^{II} ions. It was shown in the literature that the moment of the Co^{II} ions are much influenced by the variation of the actual local symmetry of their 6-fold coordination site [35]. Moreover, the distribution between Co^{II} and Co^{III} ions within the layers is not predictable and could vary as a function of the stoichiometry, due for instance to clustering effects [36]. It is noteworthy that the sample oxidized 60 h under air exhibits a steep decrease of the magnetization versus field at the inversion of the sign of the applied field (Fig. SI2e). This behavior is characteristic of fine particles behaving as monodomains which rotates with the applied magnetic field due to magnetic torque. To overcome this issue, we measured the magnetization versus field variation on a sample immobilized in eicosane. As expected, the torque did not occur then and it was possible to evaluate a coercive field of 600 Oe. This feature was not observed for the other samples.

3.3. Electrochemical properties

3.3.1. Cyclic voltammetry

$Co^{II}_{x}Co^{III}$-LDH samples were characterized with cyclic voltammetry. For divalent Cobalt cations, electrochemical reaction can be described as follow:

$$Co^{II}_{x}Co^{III} - CO_3 + yOH^- \rightleftharpoons Co^{II}_{x-y}Co^{III}_{1+y} - (OH)yCO_3 + ye^-$$

Where y is the amount of electrochemically oxidized Co^{II}. The redox mechanism is quite complex as it involves at the same time an electron transfer and charge neutralization by ion insertion or

Table 2
XRD parameters of the as-prepared $Co^{II}_{x}Co^{III}$ LDH.

Co^{III}/Co_{tot} (%)	*a* cell parameter (Å ± 0.01)	*c* cell parameter (Å ± 0.1)	$d_{spacing}$ (Å ± 0.01)
7	3.08	23.5	7.83
10	3.08	23.5	7.82
12	3.07	22.9	7.64
13	3.07	23.1	7.70
14	3.07	23.6	7.85
16	3.08	23.6	7.87

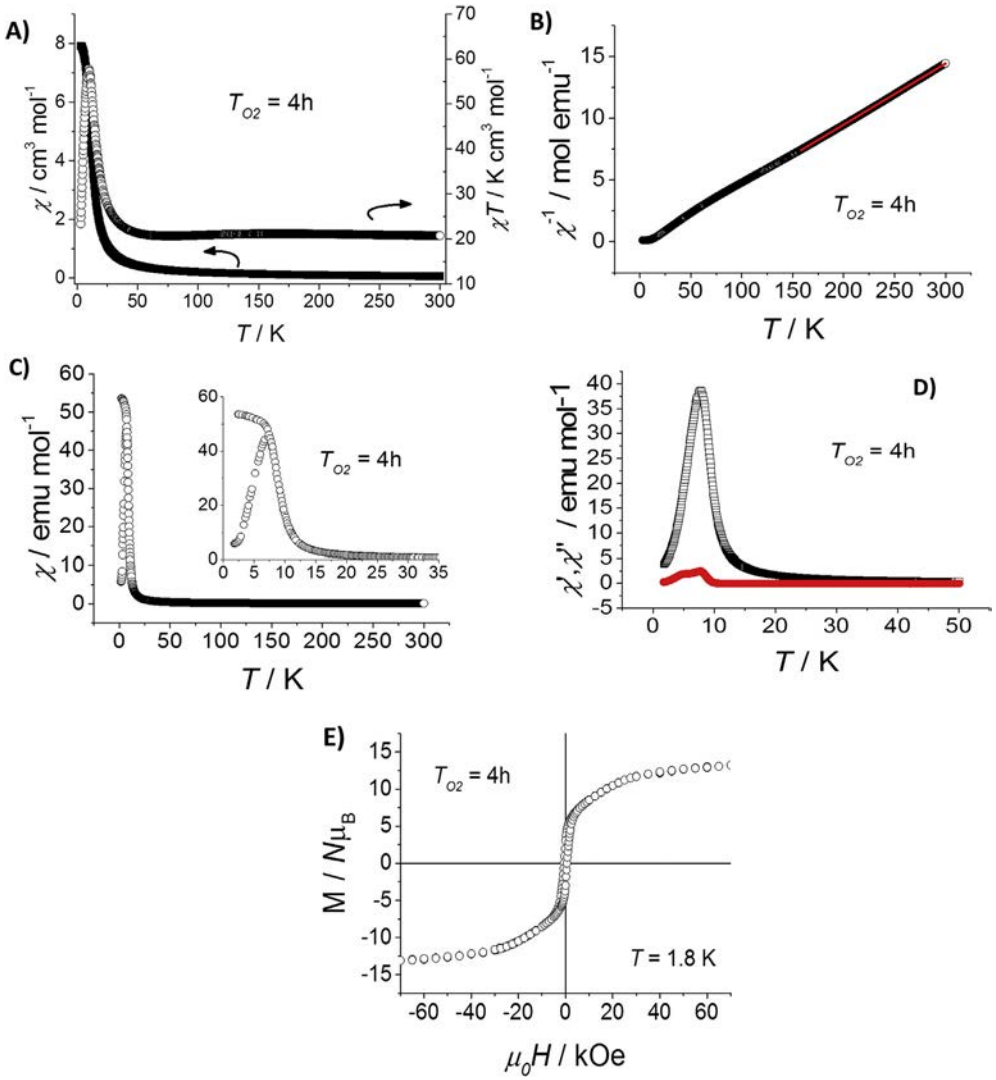

Fig. 3. Magnetic measurements for $Co^{II}_{6.7}Co^{III}$ LDH (T_{O2} = 4 h), A) thermal variation of the magnetic susceptibility and the χT product measured under applied field of 5000 Oe, B) inverse susceptibility vs T plot, C) ZFC-FC thermal variation of the magnetic susceptibility under an applied field of 100 Oe, D) AC susceptibility variation as a function of temperature (f = 83 Hz, $\mu_0.H_{AC}$ = 3.5 Oe), E) Magnetization vs Field cycle recorded at 1.8 K.

deinsertion (hydroxide insertion or proton loss). The electrochemical reaction is thus under diffusional regime control [16]. All samples exhibit a well-defined anodic peak and the associated cathodic peak with a potential separation of about 200 mV (Fig. 4A), informing on the quasi-reversible oxidation process of Co^{II} located into the LDH layer [21]. However, the shape and intensity of such response on the voltammograms were found to depend on the synthesis conditions (T_{O2}). In term of electrochemical efficiency, the integration of the anodic peak recorded at low scan rate ($v = 5$ mV s^{-1}) showed that the charges (Q_a) raised up for T_{O2} of 2 h and then decreased for longer oxidation time (Fig. 4B). The number of moles of oxidized metal cations (n* of Co^{II}) during one potential sweep was estimated from the relation $Q_a = 1e^-.F.n^*$. According to the formulae (Table 1) and the total amount of LDH coated onto the electrode surface, the efficiency of the electrochemical oxidation process was addressed, i.e. percentage of Co^{II} involved, that corresponds to a maximum value of 39% at T_{O2} = 2 h (Co^{III}/Co_{tot} = 12%, Table 4).

Table 3
Magnetic characteristics of the $Co^{II}_xCo^{III}$ LDH samples.

T_{O2} (h)	Co^{III}/Co_{tot} (%)	C (K cm³ mol^{-1})	θ (K)	T_C (K)	Hc (Oe)	Ms (μ_B)	Ms/Co^{II} (μ_B)	C/Co^{III} (K cm³ mol^{-1})
2	12	21.9	−0.2	7.15	518	12.7	1.4	2.4
60[a]	12	15.2	3.1	7.34	600[b]	9.0	1.2	2.1
4	13	20.2	8.3	7.79	602	13.2	2.0	3.0
6	14	11.8	1.8	7.46	707	7.1	1.1	1.9
8	16	12.3	5.2	7.63	467	7.4	1.4	2.3

[a] This compounds is the analog obtained by TOR in air during 60 h (see text).
[b] Measured on sample immobilized in eicosane (see text).

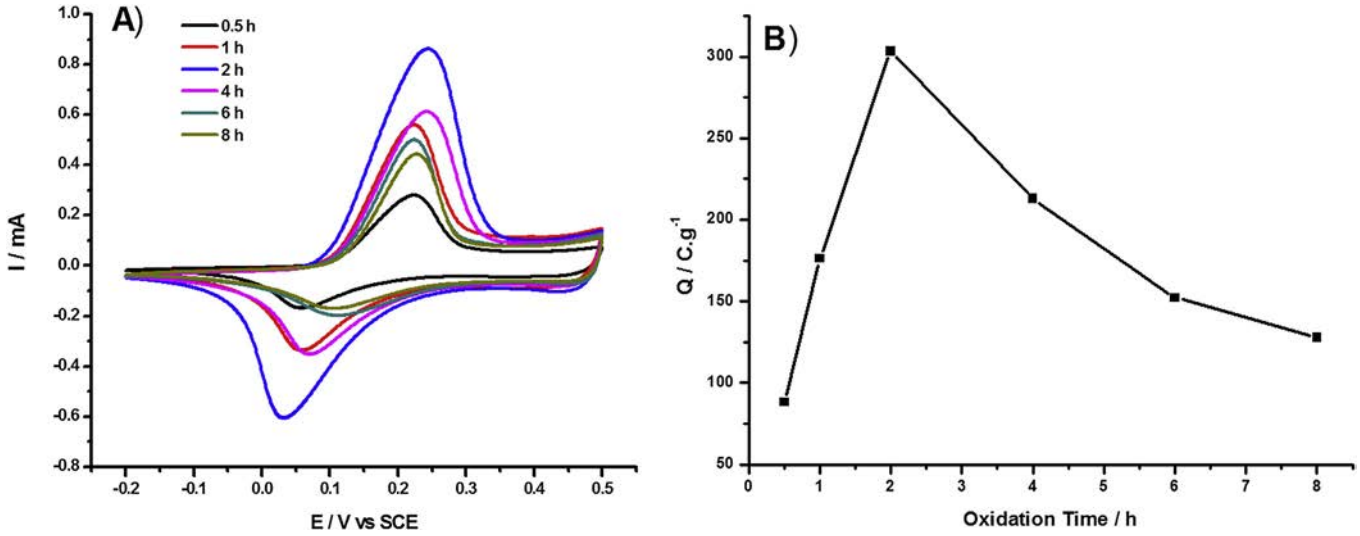

Fig. 4. A) Voltammogramms of $Co^{II}_xCo^{III}$ LDH in 0.1 M KOH ($v = 5$ mV s^{-1}). B) Evolution of Q_a as a function of sample composition.

Table 4
Electrochemical characteristics of $Co^{II}_xCo^{III}$ LDH.

Co^{III}/Co_{tot} (%)	n* Co^{II} (%)	Charge capacity ($F.g^{-1}$) at 1 A g^{-1}	Discharge capacity ($F.g^{-1}$) at 1 A g^{-1}	Coulombic efficiency (%)[a]
7	10	350	155	45
10	22	475	215	45
12	39	1015	545	54
13	27	820	420	51
14	20	570	275	48
16	17	400	170	43

[a] Calculated as discharge/charge capacities ratio.

3.3.2. *Electrochemical Impedance Spectroscopy*

To relate the electrochemical process to the modifications occurring in conductivity, EIS measurements were performed at open circuit potential after electrochemical cycling (ten cycles) (OCP_f). In the 25 mHz−100 kHz frequency range, the experimental spectra of $Co^{II}_xCo^{III}$-LDH oxidative phases displayed a quasi-straight line (Fig. 5A). Impedance data were fitted using an equivalent circuit model (see supporting information and inset Fig. 5A) taking into account the representation of pseudo-capacitance with two constant-phase components (CPE_{et} and CPE_d) and the electrolyte resistance. The evolutions of the capacity values for CPE_{et} and CPE_d were found to be coherent with a maximum value for the sample

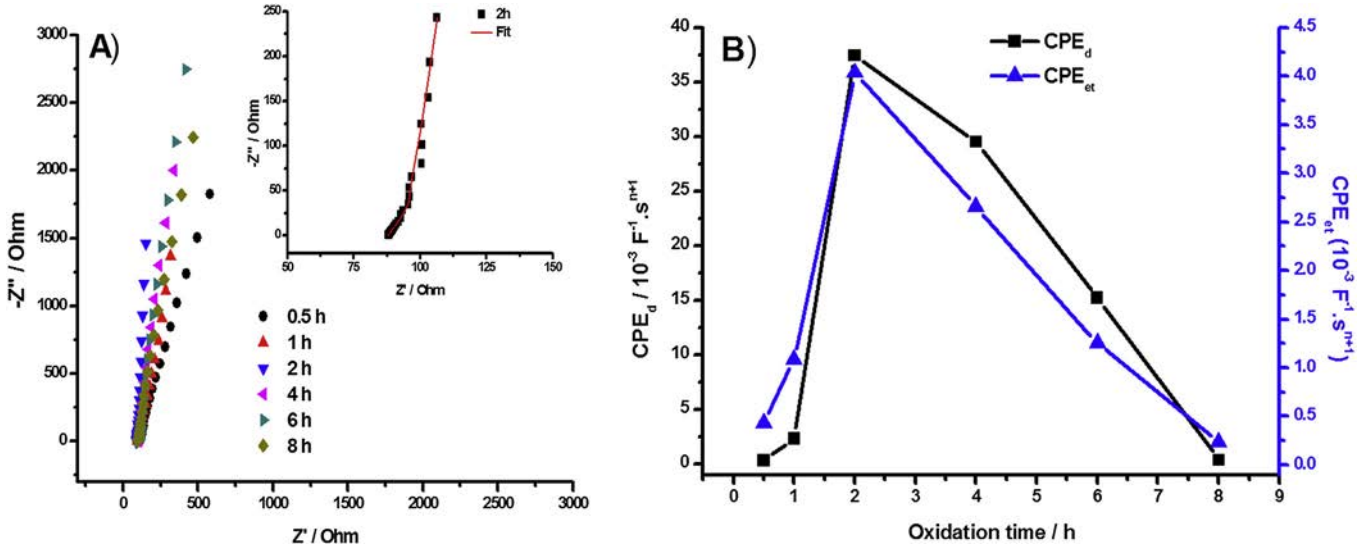

Fig. 5. A) Experimental EIS spectra of $Co^{II}_xCo^{III}$ LDH and (inset) fit of the experimental data with equivalent circuit in case of $T_{O2} = 2$ h. B) Evolution of CPE_d and CPE_{et} as a function of sample composition.

$Co^{II}_{7.3}Co^{III}$ LDH (T_{O2} = 2 h) (Fig. 5B).

3.3.3. Galvanostatic cycling with Potential limitation

Applying GCPL electrochemical technique over a potential window between 0.1 and 0.45 V/SCE and different current densities from 0.5 to 50 A.g^{-1}allows then a Ragone representation displayed for charge and discharge and representing on a power density (W.kg^{-1}) *vs* an energy density (Wh.kg^{-1}) [37] scale (Fig. 6B and B′). As exemplified at a current density of 1 A g^{-1} (Table 5 and Fig. 6A and A′) better capacitive properties were reached for $Co^{II}_{7.3}Co^{III}$-

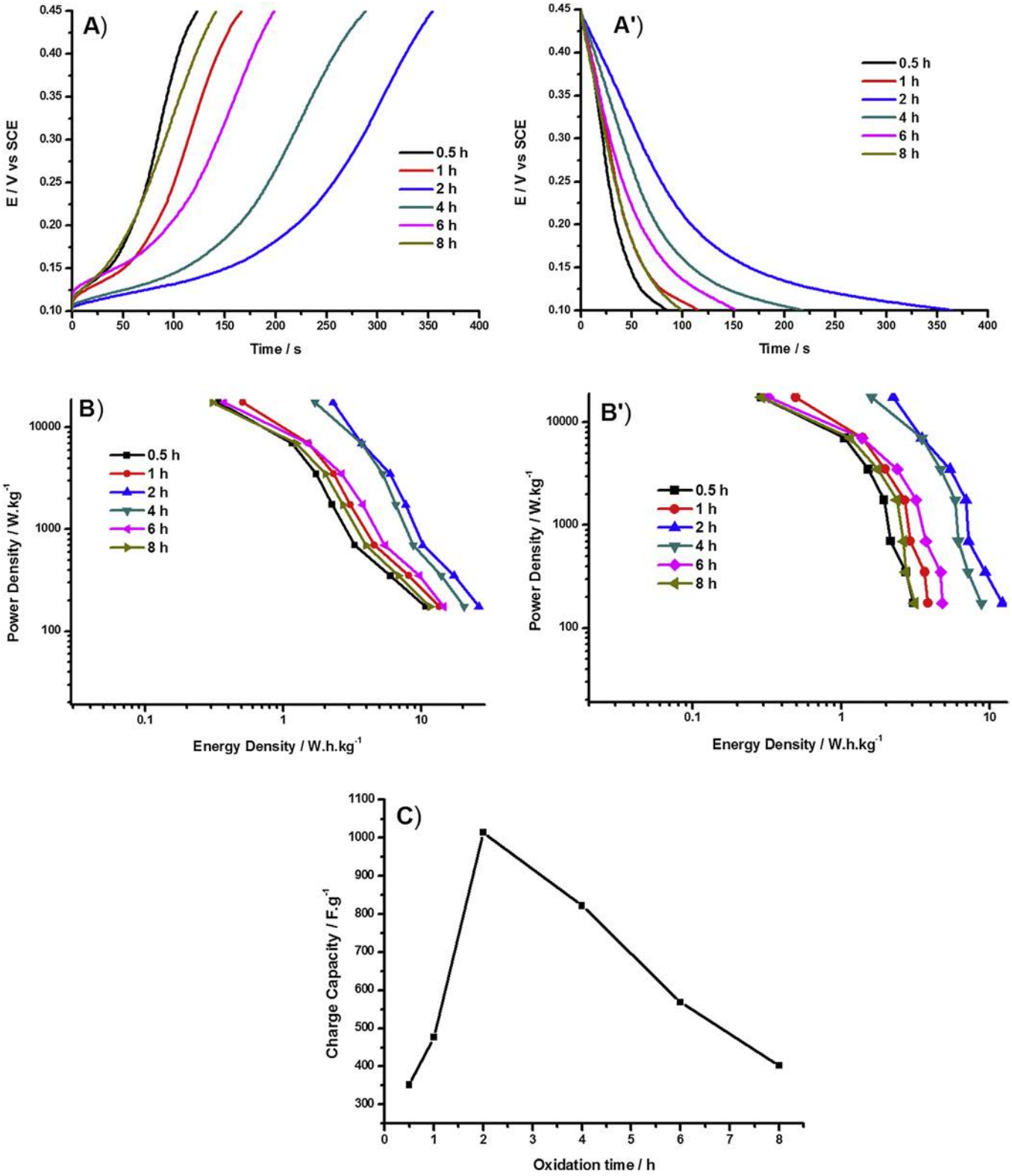

Fig. 6. A) Charge and A′) Discharge curves at 1 A g^{-1}. B) Ragone plots for charge and B′) Discharge of $Co^{II}_{x}Co^{III}$ LDH. C) Evolution of charge capacity as a function sample composition.

Table 5
Results obtained at different current densities for $Co^{II}_{7.3}Co^{III}$ LDH ($T_{O2} = 2$ h).

Current density (A.g^{-1})	Charge capacity (F.g^{-1})	Discharge capacity (F.g^{-1})	Coulombic efficiency (%)
0.5	1540	715	46
1	1015	550	54
2	605	425	70
5	455	405	89
10	350	315	91
20	220	205	94
50	135	130	97

LDH ($T_{O2} = 2$ h) (Fig. 6C). At a current density of 0.5 A g^{-1}, $Co^{II}_{7.3}Co^{III}$ LDH ($T_{O2} = 2$ h) exhibited a capacity as high as 1540 F g^{-1} and sustained 135 F g^{-1} at high current density of 50 A g^{-1}. The Ragone plots (Fig. 6B and B′) for charge demonstrated high energy density at low and high power densities up to 26.2 W h kg^{-1} at 175 W kg^{-1} and 2.29 W h kg^{-1} at 17.5 kW kg^{-1} but supplying only 12.1 W h kg^{-1} at 175 W kg^{-1} and 2.23 W h kg^{-1} at 17.5 kW kg^{-1} for the discharge, this underlined a limit of the material at low current density. Indeed, the net capacitance balance between cathodic and anodic sweep, i.e. the Coulombic efficiency, was found to depend on the applied current density, this yielding a variation between 45% at 0.5 A g^{-1} and 97% at 50 A g^{-1}.

The cyclability of the materials was evaluated by doing 100 cycles at 1 A g^{-1} and 300 cycles at 2 A g^{-1} (Fig. 7). As already reported for similar materials deposited as thin films without addition of any electronic percolation or binding agents [13], the loss of capacity is quite significant with 10% of capacity loss after 300 cycles at 2 A g^{-1} and almost 30% after 100 cycles at 1 A g^{-1}. In more details, a rapid fading in the first ten cycles is followed by a small loss of capacity. Both phenomena in time are found to be dependent of the cycling rate. For the second loss, constant decays of capacitance in time of 2 and 0.15 F g^{-1} cycle^{-1} were found under 1 and 2 A g^{-1}, respectively. This clearly indicates that the electrode elaboration has to be optimized to avoid film deterioration upon cycling, most probably due to its progressive cracking in absence of binding agent, having as a consequence its loss of integrity in terms of electrons input/withdraw diffusing at the electrode material.

4. Discussion

A topochemical oxidative reaction in air [13] during 60 h yielded a similar Co^{III}/Co_{tot} ratio than in the compound obtained with oxygen for $T_{O2} = 2$ h. Such Co^{III}/Co_{tot} molar percentage of around 12% within the LDH layer was found to be an optimum value as a function of cation oxidation state.

Hence the electrochemical properties of both $Co^{II}Co^{III}$-LDH were compared (Table 6). It is also interesting to compare with previous results on CoAl-LDH, in which 10% of Co^{II} within the layers were involved in the electrochemical oxidative process [21]. This percentage was here increased up to 28 or 39% for $Co^{II}Co^{III}$-LDH prepared in air or oxygen atmosphere, respectively (Table 5). Such high percentage underlines an efficient electrochemical oxidation of Co^{II} in monometallic LDH, associated to a significant increase in pseudocapacitive behavior. EIS measurements showed that the capacities associated to an electronic transfer into the layers (CPE_{et}) were of the same order of magnitude for both compounds and 30-fold higher than for the value for previously reported CoAl–CO_3 (0.11×10^{-3} F^{-1} s^{n-1}) [13]. However one can notice that the capacity linked with diffusion (CPE_d) was also similar for $Co^{II}Co^{III}$-LDH prepared either by air or O_2 oxidation. This can be explained by the presence of intercalated CO_3^{2-} anions in both cases inducing similar diffusion processes for charge counterbalanced by hydroxide anions during electrochemical oxidation.

Regarding performances, the charge capacities were found to be as high as ≈1500 F g^{-1} at a current density of 0.5 A g^{-1}, making

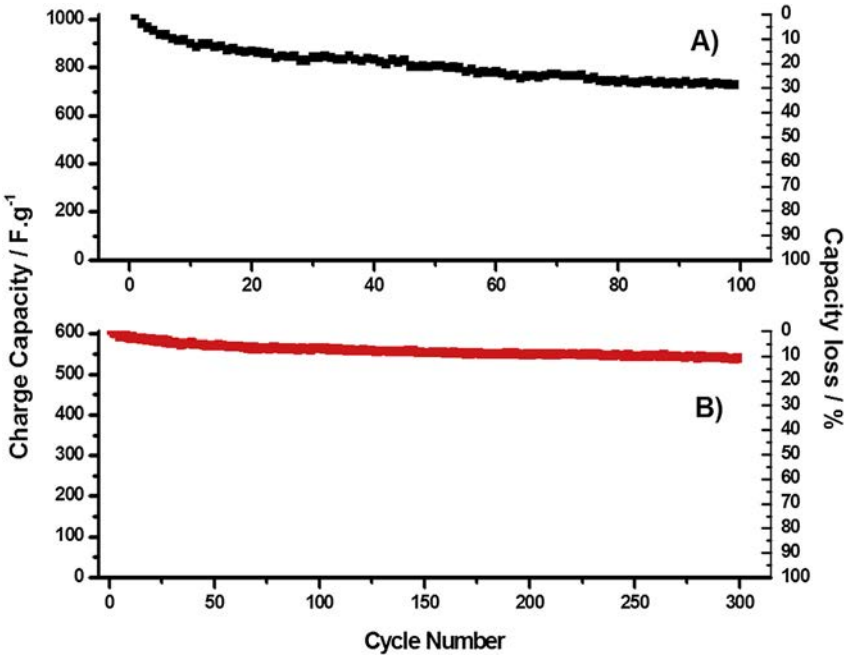

Fig. 7. Evolution of charge capacity upon cycling for $T_{O2} = 2$ h after A) 100 cycles at 1 A g^{-1} and B) 300 cycles at 2 A g^{-1}.

Table 6
Performance between $Co^{II}_xCo^{III}$ LDH prepared under oxygen atmosphere (T_{O2} = 2 h) or air atmosphere (T_{air} = 60 h).

Condition		2 h Under O_2 atmosphere	60 h Under air atmosphere
Co^{III}/Co_{tot} (%)		12	12
n* Co^{II} (%)		39	28
CPE_{et} (10^{-3} $F^{-1}.s^{n+1}$)		4.04	3.27
CPE_d (10^{-3} $F^{-1}.s^{n+1}$)		37.4	26.3
Q_{tot} ($C.g^{-1}$)		320	295
Q_{out} ($C.g^{-1}$)		120	88
Charge capacity ($F.g^{-1}$)	0.5 A g^{-1}	1540	1480
Net balance (%)		46	23
Charge capacity ($F.g^{-1}$)	50 A g^{-1}	135	20
Net balance (%)		97	100

them in the highest capacitance value never reported for pure LDH materials [2]. Moreover under high current density (50 A g^{-1}), the oxygen synthesized LDH sustained a capacitance of 133 F g^{-1} (Table 6), thus demonstrating the benefit of O_2 oxidation for the capacitive properties recorded for fast charge process. Such difference may be explained by an exposed external surface for O_2 oxidative phase, as suggested by the high value of CPE_d component in EIS measurement. This can be confirmed regarding the total charge value (Q_{tot}), which is proportional to the entire active layer, estimated from the extrapolation of Q_a at $v \rightarrow 0$ on a plot Q_a^{-1} *vs* $v^{½}$ and the outer charge Q_{out} at $v \rightarrow \infty$, which is proportional to the outer active surface, extrapolated from the Q_a *vs* $v^{-1/2}$ plot [38]. A higher Q_{out} value was found for the O_2 oxidative product compared to the air treated analogue (Table 6) whereas Q_{tot} is almost the same for the two compounds. This difference demonstrates that, at high current density where only double layer capacity phenomenon is involved in the capacitive process, O_2 oxidative product exhibits more surface and can store more charges. On the contrary, at low current density where the faradaic capacitive process is predominant, the two compounds exhibit almost the same capacitive properties.

To have an insight on the surface and morphology, SEM images of the two samples were recorded (Fig. 7). It appears that in the case of the T_{O2} = 2 h LDH, we observed a higher heterogeneity in shape and size of the particles than in the air oxidative LDH, with some hexagonal platelets with diameters around 1 μm (Fig. 8A and B) along with sand rose - like aggregates. Conversely, the LDH obtained in air exhibits a more amorphous morphology with micrometer sized blocks observed at low magnification of 5000 (Fig. 8C) which are found to be composed of very small particles of diameters lower than 50 nm when using higher magnification (Fig. 8D). This is consistent with the fact that the surface charge storage between the two samples is probably different and directly linked with the synthesis conditions. This observation is also supported by the magnetic properties as seen previously. The smaller particles obtained using synthesis under air leads to smaller magnetic particles behaving as monodomains.

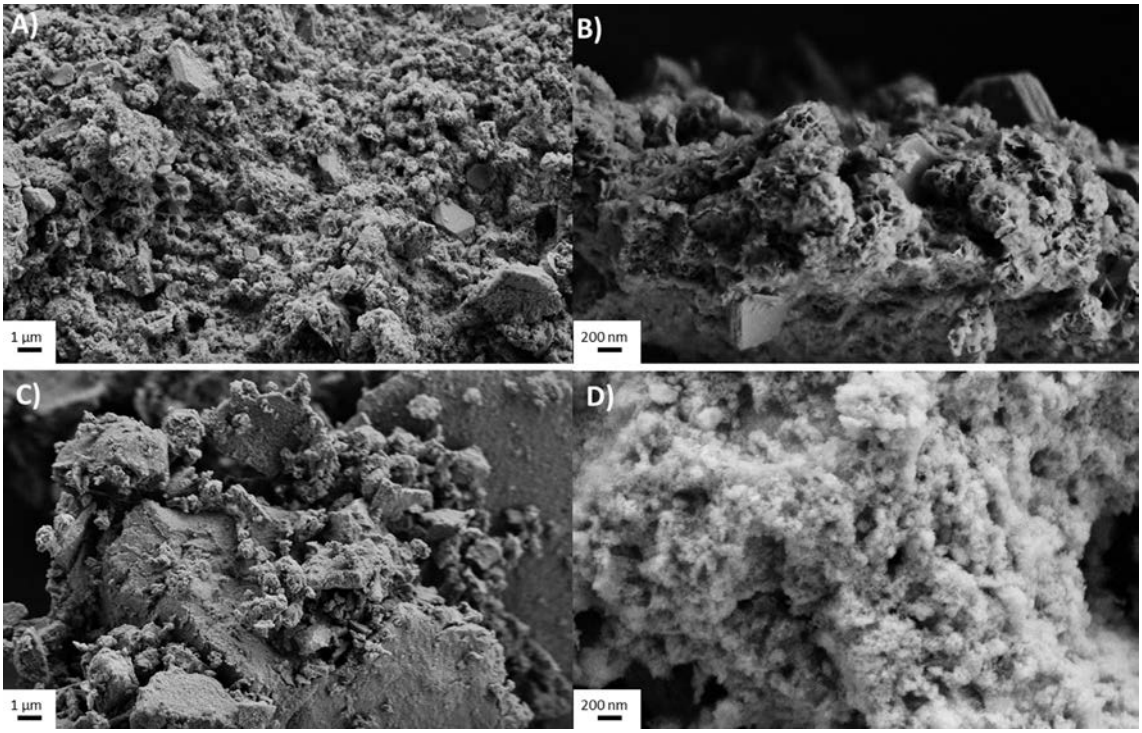

Fig. 8. SEM images of CoIICoIII LDHs obtained by oxidation under oxygen (2 h) with magnification of A) 5000 and B) 25,000 and obtained by oxidation under air with magnification of C) 5000 and D) 25,000.

5. Conclusion

In this paper, we have shown that using pure oxygen instead of air for TOR to obtain monometallic $Co^{II}_{x}Co^{III}$-CO_3 LDHs allows to significantly reducing the synthesis time necessary to reach the same Co^{III}/Co_{tot} ratio (2 h *vs* 60 h). The structure, magnetic and electrochemical properties of the samples obtained using the two different oxidizing agents were found to be quite similar. Yet, much longer oxidative treatment performed under air was found to produce fine particles behaving as mono-magnetic domains, as revealed by torque of the powder sample with inversion of field in low-temperature magnetization versus field curve. On the contrary, compounds after O_2-TOR do not display such features. Capacities as high as 1540 F g^{-1} at 0.5 A g^{-1} and 135 F g^{-1} at high current density of 50 A g^{-1} were obtained for the sample obtained with $T_{O2} = 2$ h. This confirms that these monometallic LDH can be used as promising materials for the elaboration of capacitive devices as supercapacitors.

References

[1] S. Chen, W. Xing, J. Duan, X. Hu, S.Z. Qiao, J. Mater. Chem. A (2013).
[2] C. Mousty, F. Leroux, Recent Pat. Nanotechnol. 6 (2012) 174–192.
[3] J. Fang, M. Li, Q. Li, W. Zhang, Q. Shou, F. Liu, X. Zhang, J. Cheng, Electrochim. Acta 85 (2012) 248–255.
[4] T. Yan, R. Li, Z. Li, Mater. Res. Bull. 51 (2014) 97–104.
[5] E. Scavetta, B. Ballarin, C. Corticelli, I. Gualandi, D. Tonelli, V. Prevot, C. Forano, C. Mousty, J. Power Sources 201 (2012) 360–367.
[6] S.B. Kulkarni, A.D. Jagadale, V.S. Kumbhar, R.N. Bulakhe, S.S. Joshi, C.D. Lokhande, Int. J. Hydrog. Energy 38 (2013) 4046–4053.
[7] G. Abellan, J.A. Carrasco, E. Coronado, J. Romero, M. Varela, J. Mater. Chem. C 2 (2014) 3723–3731.
[8] M.-Q. Zhao, Q. Zhang, J.-Q. Huang, F. Wei, Adv. Funct. Mater. 22 (2012) 675–694.
[9] J. Zhao, J. Chen, S. Xu, M. Shao, D. Yan, M. Wei, D.G. Evans, X. Duan, J. Mater. Chem. A 1 (2013) 8836–8843.
[10] X. Liu, C. Wang, Y. Dou, A. Zhou, T. Pan, J. Han, M. Wei, J. Mater. Chem. A 2 (2014) 1682–1685.
[11] J. Memon, J. Sun, D. Meng, W. Ouyang, M.A. Memon, Y. Huang, S. Yan, J. Geng, J. Mater. Chem. A 2 (2014) 5060–5067.
[12] L. Zhang, J. Wang, J. Zhu, X. Zhang, K. San Hui, K.N. Hui, J. Mater. Chem. A 1 (2013) 9046–9053.
[13] P. Vialat, C. Mousty, C. Taviot-Gueho, G. Renaudin, H. Martinez, J.-C. Dupin, E. Elkaim, F. Leroux, Adv. Funct. Mater. 24 (2014) 4831–4842.
[14] Z.P. Xu, H.C. Zeng, Int. J. Inorg. Mater. 2 (2000) 187–196.
[15] Z.P. Xu, H.C. Zeng, Chem. Mater. 12 (2000) 2597–2603.
[16] P. Vialat, F. Leroux, C. Mousty, J. Solid State Electrochem. (2014) 1–9.
[17] R. Ma, K. Takada, K. Fukuda, N. Iyi, Y. Bando, T. Sasaki, Angew. Chem. Int. Ed. 47 (2008) 86–89.
[18] B. Zapataa, P. Boschb, G. Fetterc, M.A. Valenzuelac, J. Navarretea, V.H. Larab, Int. J. Inorg. Mater. 3 (2001) 23–29.
[19] E. López-Salinas, M. García-Sánchez, M.L. Ramón-García, I. Schifter, J. Porous Mater. 3 (1996) 169–174.
[20] A. Vaccari, Appl. Clay Sci. 22 (2002) 75–76.
[21] P. Vialat, F. Leroux, C. Taviot-Gueho, G. Villemure, C. Mousty, Electrochim. Acta 107 (2013) 599–610.
[22] R.L. Carlin, Magneto-chemistry, Springer-Verlag, Berlin, 1986.
[23] F.E. Mabbs, D.J. Machin, Magnetism and Transition Metal Complexes, Chapman et Hall Ltd, 1973.
[24] P. Rabu, S. Angelov, P. Legoll, M. Belaiche, M. Drillon, Inorg. Chem. 32 (1993) 2463–2468.
[25] J.-M. Rueff, N. Masciocchi, P. Rabu, A. Sironi, A. Skoulios, Chem. Eur. J. 8 (2002) 1813.
[26] J.-M. Rueff, C. Paulsen, J. Souletie, M. Drillon, P. Rabu, Solid State Sci. 7 (2005) 431–436.
[27] K. Katayama, M. Hirotsu, I. Kinoshita, Y. Teki, Dalton Trans. 43 (2014) 13384–13391.
[28] C.-H. Cho, T.-Y. Chien, J.-H. Chen, S.-S. Wang, J.-Y. Tung, Dalton Trans. 39 (2010) 2609–2614.
[29] F.A. Cotton, G. Wilkinson, Adv. Inorg. Chem., fifth ed., Wiley Interscience, John Wiley and Sons, 1988.
[30] W.E. Hatfield, Magnetic measurements, in: A.K. Cheetham, P. Day (Eds.), Solid State Chemistry - Techniques, Clarendon Press, Oxford, 1987, pp. 123–162.
[31] V. Laget, M. Drillon, C. Hornick, P. Rabu, F. Romero, P. Turek, R. Ziessel, J. Alloy. Compd. 423 (1997) 262–263.
[32] G. Abellán, E. Coronado, C. Martí-Gastaldo, A. Ribera, J.L. Jordá, H. García, Adv. Mater. 26 (2014) 4156–4162.
[33] E. Delahaye, S. Eyele-Mezui, J.-F. Bardeau, C. Leuvrey, L. Mager, P. Rabu, G. Rogez, J. Mater. Chem. 19 (2009) 6106–6115.
[34] A. Demessence, A. Yassar, G. Rogez, L. Miozzo, S. De Brion, P. Rabu, J. Mater. Chem. 20 (2010) 9401–9414.
[35] C.F. Smura, D.R. Parker, M. Zbiri, M.R. Johnson, Z.A. Gál, S.J. Clarke, J. Am. Chem. Soc. 133 (2011) 2691–2705.
[36] G. Abellán, E. Coronado, C. Martí-Gastaldo, J. Waerenborgh, A. Ribera, Inorg. Chem. 52 (2013) 10147–10157.
[37] Z. Wu, C. Xu, H. Chen, H. Yu, Y. Wu, F. Gao, Mater. Res. Bull. 48 (2013) 2340–2346.
[38] S. Ardizzone, G. Fregonara, S. Trasatti, Electrochim. Acta 35 (1990) 263–267.